JTTEE5 17:788–795
DOI: 10.1007/s11666-008-9255-4
1059-9630/$19.00 © ASM International

Effect of the Structural Scale of Plasma-Sprayed Alumina Coatings on Their Friction Coefficients

G. Darut, H. Ageorges, A. Denoirjean, G. Montavon, and P. Fauchais

(Submitted May 8, 2008; in revised form September 18, 2008)

The objective of this study is to compare the tribological properties of alumina coatings with two different structural scales, a micrometer-sized one manufactured by atmospheric plasma spraying and a sub-micrometer-sized one manufactured by suspension plasma spraying. Coating architectures were analyzed and their friction coefficients in dry sliding mode measured. Sub-micrometer-sized structured coatings present a lower friction coefficient than micrometer ones, thanks to their higher cohesion and smaller characteristic structural feature sizes.

Keywords alumina, friction, plasma spraying, sub-micrometer-sized feedstock, suspension plasma spraying, structural scale, tribology, wear

1. Introduction

Emissions of greenhouse gases (GHGs) related to anthropogenic activities are responsible for climate global warming (CGW) (Ref 1). In its last released report (Ref 2), the Intergovernmental Panel of Climate Change estimates that carbon dioxide emissions resulting from fossil fuel use are mainly responsible for GHGs (~56% of GHGs). In Western European countries, about 30% of GHGs from fossil fuel use result from car and truck transportation. Reducing those GHGs to mitigate CGW to 2 °C over this century is absolutely required to limit to the maximum possible extent impacts associated with global average temperature change. Until the deployment on a large scale of sustainable energy sources such as solid oxide-fuel cells (SOFCs) or proton exchange membrane fuel cells (PEMFCs) at horizon 2030 (Ref 3), fossil energy will remain a major source of GHGs. Reducing those emissions requires improving the engine efficiency for energy saving.

Friction is responsible for about 50% of energy loss in an automotive engine. Reducing friction within an engine is hence a major challenge that has been pursued for numerous years by major automotive companies in collaboration with technical centers.

The development 25 years ago of Nicasil-type coatings, a composite electrolytic layer made of a dispersion of micrometer-sized SiC particles embedded in a Ni matrix, constituted the first effort to meet this challenge (Ref 4). Nowadays, low carbon alloyed steel layers are applied by thermal spraying (Ref 5, 6). The improvement of new sliding layers is done nowadays following three complementary directions:

1. The decrease in the material architecture scale to reach sub-micrometer-sized or nanometer-sized scales. Numerous developments aim hence at manufacturing composite micrometer-sized layers with embedded nanometer-sized particles by electrolytic (Ref 7) or thermal spraying routes or at manufacturing layers structured at the nanometer scale (Ref 8). In these both cases, published works have demonstrated significant improvements in coatings properties (wear resistance, toughness, etc.) (Ref 9-12).
2. The replacement of the metallic matrix by a ceramic matrix in order, on the one hand, to increase the local operating temperature and, on the other hand, to limit the emission of heavy metal dusts resulting from abrasion during sliding (Ref 13).
3. Less lubricated systems since synthetic oils, the most used ones in recent engines, are synthesized from fossil fuels. For example, the annual consumption of engine oil in France was 341,824 tons in 2006 (decrease of 4% compared to the previous year) to be added to several hundreds of tons of additives (Ref 14). This represents a challenge in recycling

This article is an invited paper selected from presentations at the 2008 International Thermal Spray Conference and has been expanded from the original presentation. It is simultaneously published in *Thermal Spray Crossing Borders, Proceedings of the 2008 International Thermal Spray Conference*, Maastricht, The Netherlands, June 2-4, 2008, Basil R. Marple, Margaret M. Hyland, Yuk-Chiu Lau, Chang-Jiu Li, Rogerio S. Lima, and Ghislain Montavon, Ed., ASM International, Materials Park, OH, 2008.

G. Darut, H. Ageorges, A. Denoirjean, G. Montavon, and **P. Fauchais**, SPCTS-UMR CNRS 6638, Faculty of Sciences, University of Limoges, 123 Avenue Albert Thomas, 87060 Limoges Cedex, France. Contact e-mail: ghislain.montavon@unilim.fr.

those products after usage (278,820 tons of used engine oils recycled in 2006 in France (Ref 14)). Decreasing their consumption would reduce their environmental impact.

In this context, thermal spraying appears as a pertinent process since it permits processing of a wide range of feedstock, in terms of composition (ceramic, alloys, polymers), architecture (composite powders), and sizes (from micrometer-sized to nanometer-sized).

The primary objective of this work is to estimate the effect of the structural scale of plasma-sprayed coatings on some of the tribological properties in the dry mode, particularly the friction coefficient.

Alumina was selected as a demonstrative material. Indeed, alumina is used for wear-resistant layers and it is not a material suitable for friction layers (as it exhibits poor friction coefficients whatever the counter material nature). The objective here is to discriminate the effect of the structural scale rather than developing layers with low friction coefficients. In order to study the behaviors of structures exhibiting two significantly different scales, two plasma spray processes were selected: atmospheric plasma spraying (APS) was implemented to manufacture alumina coatings at a micrometer-sized scale while suspension plasma spraying (SPS) was implemented to manufacture alumina coatings at a sub-micrometer-sized scale. There were almost two orders of magnitude difference in the scale of the studied structures due to the selected feedstock average diameters (d_{50} of the particle size distributions), taken as reference to quantify the structural scale.

SPS is a technology that permits the deposition of layers thinner and finer than those resulting from conventional APS. Compared to conventional coatings, those manufactured from suspensions exhibit quite interesting features such as the absence of lamella boundaries and cracks and porous microstructures with void dimension of the same order or lower than the one of the feedstock (Ref 15, 16). In this process, a stabilized suspension, made of a liquid, solid particles, and a dispersant, is injected within the plasma flow. The liquid is very quickly vaporized and the individual particles, or the particle agglomerates, depending on the average size of the solid feedstock, are heated and simultaneously accelerated toward the substrate surface where they impact, spread, and solidify, analogously in a first approximation to larger particles, to form a layer (Ref 17, 18). Compared to plasma spraying of micrometer-sized particles (i.e., conventional plasma spraying), SPS exhibit several major differences (Ref 19):

1. SPS exhibits a more pronounced sensitivity to arc root fluctuations, requiring specific operating parameters in order to operate the spray gun in its take over mode to avoid inhomogeneous processing of the suspension by the plasma which induces heterogeneity in the coating structure.
2. The spray distance in SPS is shorter (30-40 mm) since small particles decelerate much faster than bigger ones.
3. In SPS, a higher thermal flux is transmitted from the plasma flow to the substrate, between 5 and 10 times than the heat flux transmitted in conventional plasma spraying (from 7 to 15 MW m^{-2} compared to 1.5 to 2 MW m^{-2}, average values).

2. Experimental Protocols

2.1 Spray Process and Related Parameters

Table 1 summarizes the operating parameters for both APS and SPS processes.

SPS layers were sprayed implementing a d.c. stick-cathode plasma torch developed at SPCTS equipped with a 5-mm nozzle internal diameter and operated with an arc current intensity of 600 A with a binary Ar-He (30-30 slpm) plasma gas mixture. The injection system was made of a stainless steel injector at the tip of which a calibrated diaphragm with an internal diameter of 150 μm was mounted. The suspension to be sprayed was stored in pressurized tanks and, according to the air pressure applied in the tank, the velocity of the suspension at the injector exit was 25 m s^{-1}. The suspension was made of α-Al_2O_3 P152 SB ($d_{50} = 0.3$ μm) feedstock supplied by Alcan (Saint-Jean de Maurienne, France), with a mass percentage of 10% in pure ethanol. The spray velocity (relative velocity between the substrate and the plasma torch) was 1 m s^{-1} and the scanning step 10 mm per pass, whereas the spray distance (SD) was 30 or 40 mm.

APS layers were sprayed with the same spray torch equipped with a 7-mm internal diameter nozzle. In this case, the plasma forming gas mixture was Ar-H_2 (46-14 slpm) and the arc current intensity 600 A. Powders were injected perpendicularly to the plasma jet axis with argon as carrier gas through a 1.8-mm internal diameter injector. The feedstock was α-Al_2O_3 typified Medipure ($d_{50} = 36$ μm) fused and crushed powder supplied by Medicoat (Delle, France).

For both processes, specimens for microstructural characterizations were button-type substrates made of low carbon steel 25 mm in diameter and 20 mm in thickness.

Table 1 Main spray operating parameters for APS and SPS

Operating parameters	APS	SPS
Anode internal diameter, mm	7	5
Primary plasma forming gas flow rate, slpm	46 (Ar)	30 (Ar)
Secondary plasma gas flow rate, slpm	14 (H_2)	30 (He)
Arc current intensity, A	600	600
Plasma mass enthalpy, MJ kg^{-1}	14	12
Feedstock carrier	Ar (gas)	Et-OH (liquid)
Feedstock carrier flow rate, slpm	5	n.a.
Injector internal diameter, mm	1.80	0.15
Spray distance (SD), mm	110	30/40
Spray velocity, m s^{-1}	1	1
Scanning step, mm per pass	6	10

Specimens for tribological characterizations were made of the same low carbon steel 50 mm in diameter and 5 mm in thickness. Substrates were polished to reach a specular surface finishing (i.e., average roughness ranging from 0.3 to 0.4 μm) for the SPS process and grit-blasted for APS in order to get an average roughness (R_a) of about 5 μm and a peak-to-valley ratio (R_z) of about 30 μm (R_z). Prior to spraying, they were degreased by immersion in ethanol with ultrasonic treatment.

2.2 Coating Characterization Techniques

Samples were cross-sectioned using a diamond saw, mounted in epoxy rings (vacuum impregnation), and polished using conventional polishing protocols consisting of pre-polishing using SiC papers and polishing using diamond slurries. Polished coating cross sections and fracture surfaces were observed using scanning electron microscopy (SEM) and field-emission scanning electron microscopy (FESEM). Image analysis was implemented to quantify the porosity level and crack network orientation (Ref 20).

A ball-on-disk (BOD) tribometer (CSM Instruments, Lausanne, Switzerland) was used to quantify the coating friction coefficients. A previous study established reference operating parameters as follows: α-Al_2O_3 (sintered) ball of 6 mm in diameter, 2 N load, relative speed of 0.1 m s^{-1}, and sliding distance of 1500 m. The test was operated in the dry mode and the wear scraps (i.e., third body) were constantly removed by an air jet located behind the contact point. Since as-sprayed layers exhibited significantly different surface roughnesses (both R_a and R_z, see Sect 3.1), coating surfaces were polished prior to BOD tests until the average surface roughness was in the order of a micrometer for all of them (see Sect 3.2). The surface polishing was performed using conventional metallographic polishing protocols.

The wear profile and roughness were measured with a Dektak IIA surface profiler (Veeco Instruments, Woodbury, NY) which has a tip radius of 10 μm.

3. Results and Discussion

3.1 Coating Architectures

The average thickness of APS coatings was about 330 μm, whereas the thickness of SPS layers was 12 μm for SD = 30 mm and 15 μm for SD = 40 mm. The average roughness of as-sprayed APS coatings was about 5.07 μm ± 0.19; the average of SPS coatings only about 1.6 μm ± 0.10.

Figure 1 displays the major difference in structural scales for both APS- and SPS-sprayed coatings. The average flattening ratio of lamellae forming the APS coating is estimated to vary from 3 to 4—a common value encountered for this type of process—whereas it is estimated to vary from 1 to 2 for SPS coatings that exhibit a granular-type structure (to be compared to the conventional layered structure of APS coatings). In the two processes, the predominant bounding mechanism of the coating to the substrate is very likely mechanical anchorage. Mechanical anchorage is promoted when the substrate surface average roughness is of the same order than the lamella thickness, a few micrometers (2-4 μm) in APS coatings and a few tenths of micrometers (0.2-0.4 μm) in SPS. Consequently, coatings are manufactured by APS onto grit-blasted substrate surface and by SPS onto polished substrate surface. In the peculiar case of SPS coatings, an additional bounding mechanism could result from the development of an interphase at the substrate/coating interface made of a layer of mixed oxides developing onto the substrate surface consecutively to the high heat flux imparted by the plasma flow. Indeed, Valette et al. (Ref 21) have demonstrated in conventional plasma spraying that an interphase could be promoted by oxidation resulting in an epitaxial solidification of alumina lamellae onto an iron oxide layer itself epitaxied onto the steel substrate. Works are underway to more specifically address this mechanism in SPS.

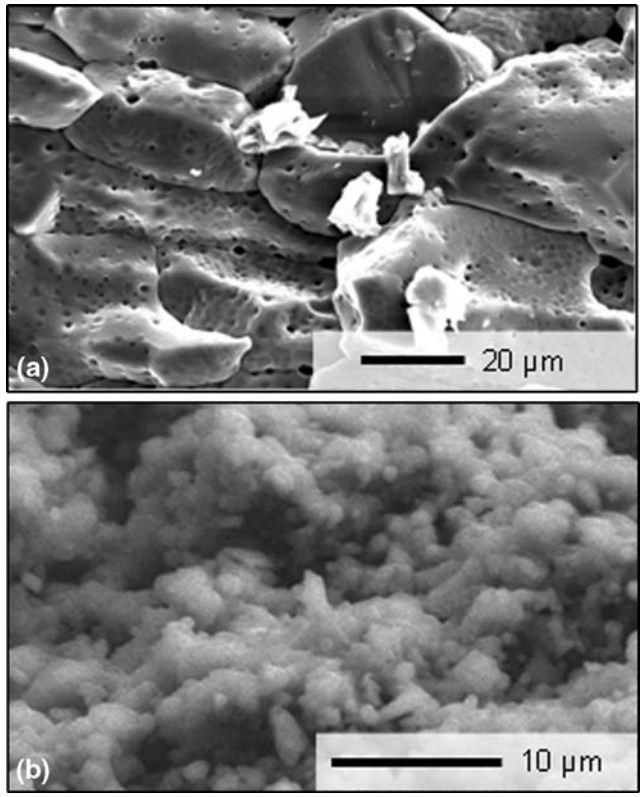

Fig. 1 Fracture surfaces of (a) micrometer-sized (APS) and (b) sub-micrometer-sized (SPS) Al_2O_3 coatings

Figure 2 displays the pore network architecture of APS and SPS coatings. They differ by their pore level: about 4% for SPS layers to be compared to about 9% for APS ones. Besides, the pore network architecture differs also since it seems to be made exclusively of voids for SPS layers whereas it is made of voids (80 vol.%) and cracks (20 vol.%), the latter consisting of interlamellar delaminations perpendicular to the spray direction (80 vol.%) and intra-lamellar cracks parallel to the spray direction (20 vol.%) for APS layers.

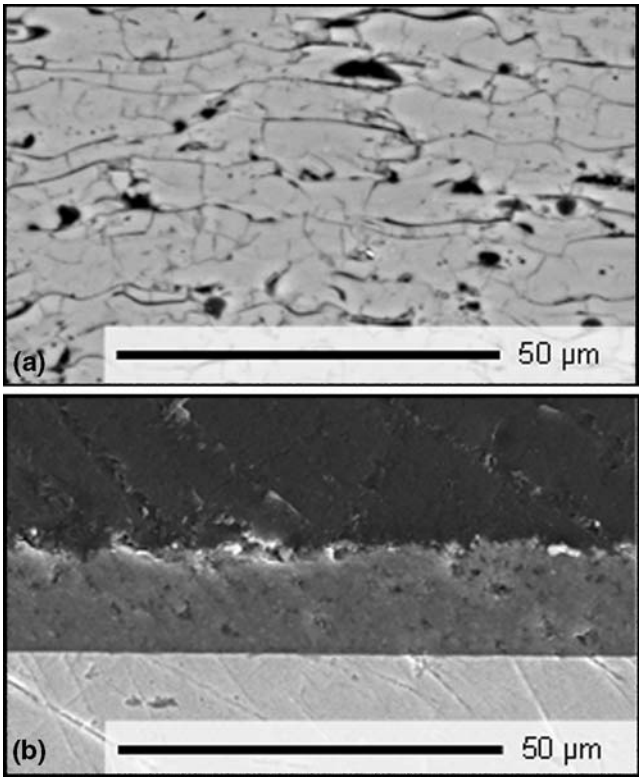

Fig. 2 Polished cross sections of (a) micrometer-sized (APS) and (b) sub-micrometer-sized (SPS) Al_2O_3 coatings presented at the same magnification

3.2 Coating Friction Coefficient

As mentioned in Sect 2.2, the differences in as-sprayed coating roughnesses required that they be polished prior to BOD tests. Tables 2 and 3 display measured values after polishing (average value and associated standard deviation of 10 randomly located measurements). R_a is the arithmetic mean of the absolute departures of the roughness profile from the mean line, R_z the maximum peak-to-valley height at the mean line, R_{sk} the skewness, R_{ku} the kurtosis, R_{Sm} the mean spacing between profile peaks at the mean line, and R_{HTp} the height of the bearing ratio of the complete profile (Ref 22).

The values differ by about 50% for R_a and R_z between SPS and APS coatings due to a polishing protocol not fully optimized at this stage. The mean spacing, R_{Sm}, is almost identical for coatings manufactured with both processes. Polished surface topologies differ mostly by their skewness and kurtosis. Polished APS coating surfaces are made of more valleys than peaks (i.e., negative skewness) while polished SPS surfaces have almost symmetrical topologies corresponding to skewness values close to zero. Polished SPS coating topologies exhibit a distribution of heights closer to the normal distribution (i.e., corresponding to a kurtosis equal to 3) compared to polished APS coating surfaces. Those characteristics lead to a bearing ratio higher for polished APS coatings compared to SPS ones.

Table 2 Roughness criteria for polished specimens

Surface parameters	APS	SPS	
		SD = 30 mm	SD = 40 mm
R_a, µm	0.71 ± 0.10	1.45 ± 0.24	1.42 ± 0.15
R_z, µm	5.77 ± 0.77	9.39 ± 1.69	8.31 ± 0.85
R_{sk}, –	−1.46 ± 0.33	0.67 ± 0.19	−0.09 ± 0.13
R_{ku}, –	7.32 ± 1.64	3.56 ± 0.77	2.55 ± 0.24
R_{Sm}, µm	57.86 ± 8.13	40.68 ± 2.28	39.68 ± 3.51
R_{HTp}, µm	1.37 ± 0.23	2.99 ± 0.54	3.16 ± 0.34

Table 3 Roughness criteria for polished specimens

Surface parameters	SPS		
	SD = 30 mm	SD = 40 mm	SD = 50 mm
R_a, µm	1.82 ± 0.14	2.57 ± 0.23	3.11 ± 0.27
R_z, µm	11.53 ± 1.02	15.26 ± 1.30	17.83 ± 1.25
R_{sk}, –	0.67 ± 0.21	0.28 ± 0.16	0.,19 ± 0.20
R_{ku}, –	3.36 ± 0.65	2.77 ± 0.23	2.64 ± 0.21
R_{Sm}, µm	48.90 ± 3.26	54.06 ± 4.85	62.61 ± 7.41
R_{HTp}, µm	3.86 ± 0.35	5.46 ± 0.56	6.64 ± 0.72

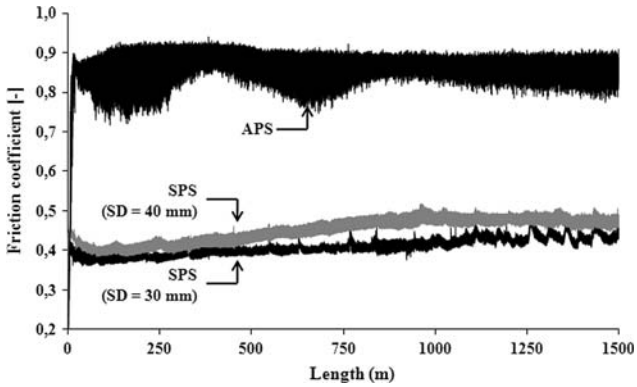

Fig. 3 Friction coefficient versus sliding distance for Al_2O_3 micrometer-sized (APS) and sub-micrometer-sized (spray distance = 30 and 40 mm) coatings (BOD, α-Al_2O_3 ball of 6 mm in diameter, 2 N load, relative speed of 0.1 m s^{-1})

Nevertheless, and in a first approximation, such differences do not play a significant role, except in the accommodation stage of the friction curves, since the roughness descriptor values vary in narrow ranges.

Figure 3 displays the evolution of coating friction coefficients versus sliding distance of micrometer-sized (APS) and sub-micrometer-sized (spray distance of 30 and 40 mm) structural scale layers. Table 4 summarizes friction coefficient average values for several ranges of sliding distance. The structural scale plays obviously a relevant role on the friction coefficient: it evolves from an average value of about 0.8 for APS coating (micrometer scale) to about 0.4-0.5 for SPS coatings (sub-micrometer scale), clearly demonstrating the benefit on tribological behavior provided by finely structured structures over larger ones.

Considering APS coatings, voids, interlamellar delaminations, and intralamellar cracks lead to weakened lamella boundaries. When a contact load is applied on the coating and because of a reduced mechanical strength, lamellae are exfoliated generating a rough surface topology. As a result, the friction force is high. Considering SPS coatings and because of a smaller grain size and the absence of apparent delaminations and cracks (Fig. 1), particles are strongly linked together. This improves the resistance to crack propagation and lamella exfoliation, as published works have shown (Ref 23, 24). Moreover, when lamella exfoliation occurs, changes in surface topology are lower in magnitude. This results in a lowered friction coefficient. This is confirmed by the lower fluctuations in friction coefficients (noise) imparted by surface heterogeneities for SPS coatings compared to APS coatings, thanks to their finer and more homogeneous structures. Concerning SPS coatings, coatings sprayed with a 30-mm spray distance show a slightly lower friction coefficient compared to the ones sprayed with a 40-mm spray distance. Figure 4 displays the evolution of coating friction coefficient versus sliding distance curves for three spray distances of SPS layers. The average friction coefficients are given in Table 5. As mentioned previously, the longer the spray distance, the lower the friction coefficient. This can be directly related to their porous architecture and cohesive strength, a shorter spray distance increasing the layer cohesion while reducing the stacking defect density, as shown by Tingaud et al. (Ref 25) (Fig. 5). In fact, for the largest spray distance, lack of cohesion leads to layer destruction at about 750 m.

Additional tests at a sliding distance of 3000 m, shown in Fig. 6 (instead 1500 m for the previous experiments), demonstrated that SPS coatings sprayed at a 30-mm distance behaved identically; that is, the friction coefficient remains equal to 0.4 with no clear evidence of wear according to Fig. 7.

Considering wear mechanisms, grooves, cracks, and a relatively rough surface topology observed for APS coatings (Fig. 8a and b) demonstrates that they have encountered severe wear. In fact, the wear mechanism is well known in this case. Lamella delamination begins with the appearance of cracks and their propagation between two lamellae. Another relevant mechanism is inter-lamellar delamination along a weak interface between successive lamellae (Ref 26), particularly when inter-lamellar delaminations develop due to particle rapid solidification (Ref 27). Of course, splat delamination is also facilitated by the presence of defects such as unmolten or semi-molten particles, voids, cracks, etc. For SPS coatings, the wear track presents no grooves nor cracks and the surface is relatively smooth (Fig. 8c and d). One explanation is the absence of lamella exfoliation but only a plastic deformation as depicted in Fig. 9. Wear occurs only at the

Table 4 Average friction coefficients for several ranges of sliding distances

Sliding distance range, m	Friction coefficient, –		
	APS	SPS (SD = 40 mm)	SPS (SD = 30 mm)
100-400	0.9	0.4	0.4
400-900	0.9	0.4	0.4
900-1500	0.9	0.5	0.4
1500-3000	n.a.	n.a.	0.4

Table 5 Average friction coefficients for several ranges of sliding distances

Sliding distance range, m	Friction coefficient, –		
	SPS (SD = 30 mm)	SPS (SD = 40 mm)	SPS (SD = 50 mm)
0-250	0.30	0.30	0.35
250-750	0.30	0.35	0.40
750-1000	0.30	0.35	n.a.
1000-1500	0.30	0.40	n.a.

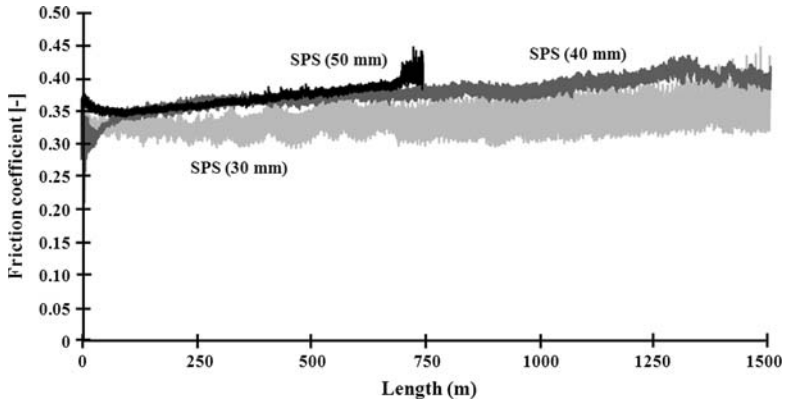

Fig. 4 Friction coefficient versus sliding distance for Al_2O_3 sub-micrometer-sized (spray distance = 30, 40, and 50 mm) coatings (BOD, α-Al_2O_3 ball of 6 mm in diameter, 2 N load, relative speed of 0.1 m s^{-1})

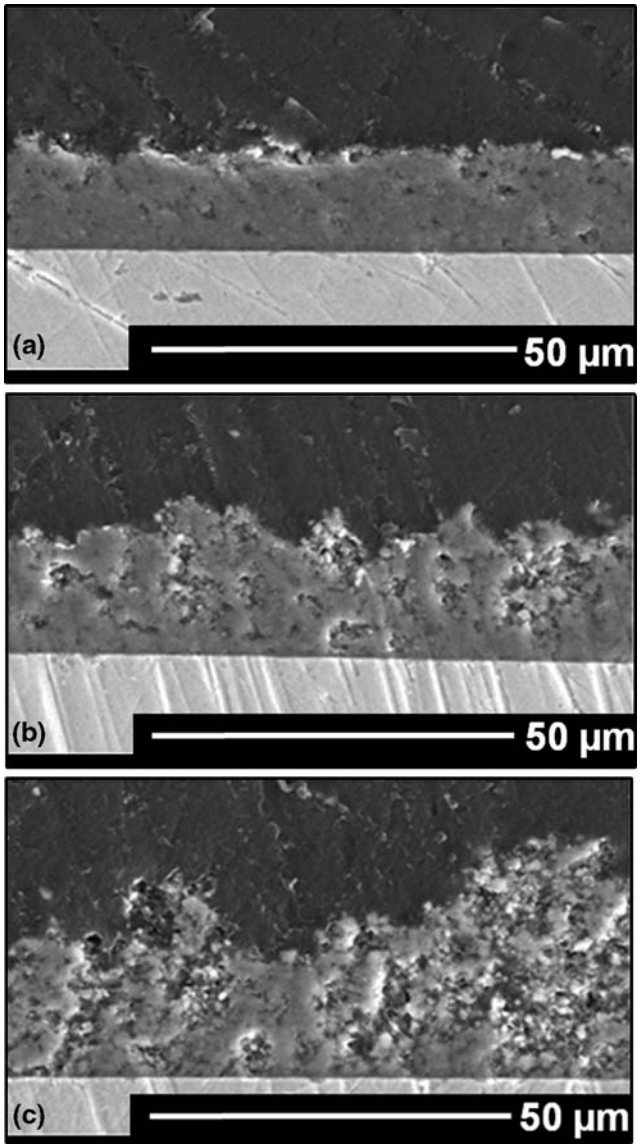

Fig. 5 Polished cross sections of sub-micrometer-sized Al_2O_3 (SPS) coatings sprayed at (a) 30 mm, (b) 40 mm, and (c) 50 mm

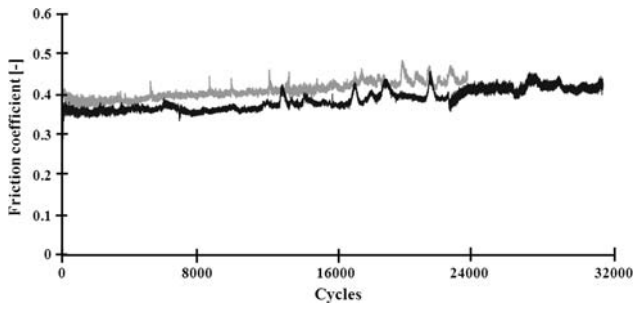

Fig. 6 Friction coefficient versus sliding distance for Al_2O_3 sub-micrometer-sized SPS (spraying distance of 30 mm) coatings for a sliding distance of 1500 and 3000 m (BOD, α-Al_2O_3 ball of 6 mm in diameter, 2 N load, relative speed of 0.1 m s^{-1})

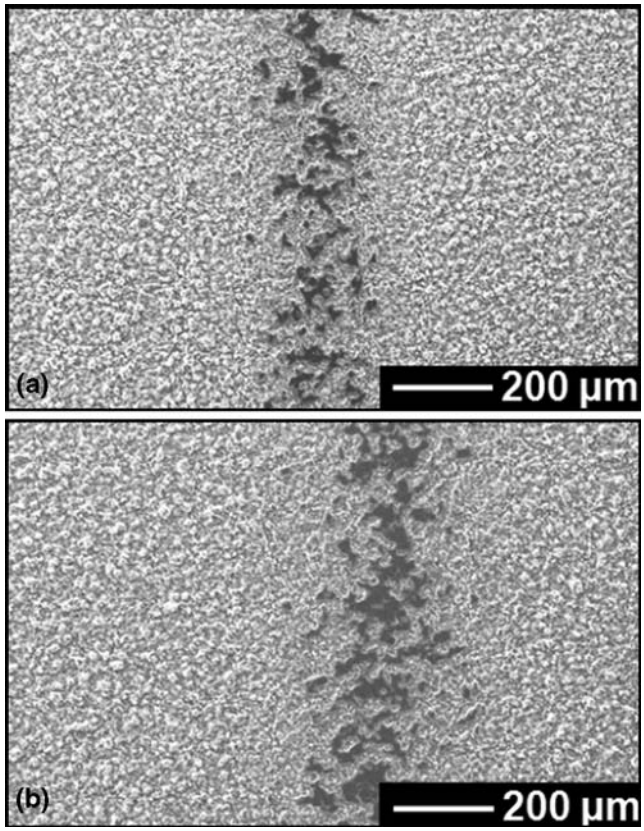

Fig. 7 Wear tracks resulting from BOD test with sub-micrometer-sized SPS (spraying distance of 30 mm) coatings for a sliding distance of (a) 1500 m and (b) 3000 m (α-Al_2O_3 ball of 6 mm in diameter, 2 N load, relative speed of 0.1 m s^{-1})

asperities, which would account very likely for the high cohesion strength between neighbor lamellae (Ref 28, 29). A published study points out that plastic deformation can permit to dissipate energy from strain (Ref 24). Besides, Lima et al. (Ref 23) have demonstrated that a thinner structure was characterized by a lower level of residual stresses due to a lower mismatch thermal expansion between coating and substrate (2-3 times). Indeed, Fig. 10 presents profiles of wear tracks for the three considered structures. The wear rate of APS coatings (micrometer-sized architecture) is significantly higher than the one of SPS coatings (sub-micrometer-sized architecture): almost 0 for SPS and 2.93×10^5 µm^3 N^{-1} m^{-1}. These results corroborate researches made on ''nano effect'' (Ref 30-32). At this stage of the experiments, no clear evidence of SPS wear has been identified as the track depth corresponds to the characteristic dimension of the surface roughness.

The behavior of SPS alumina sub-micrometer-sized coatings could be very likely extended for these specific test conditions to other oxides, such as ZrO_2 for example, until no transfer between coating and counter material (ball) occurs. The behavior of metallic coatings would be very likely very different due to such a transfer.

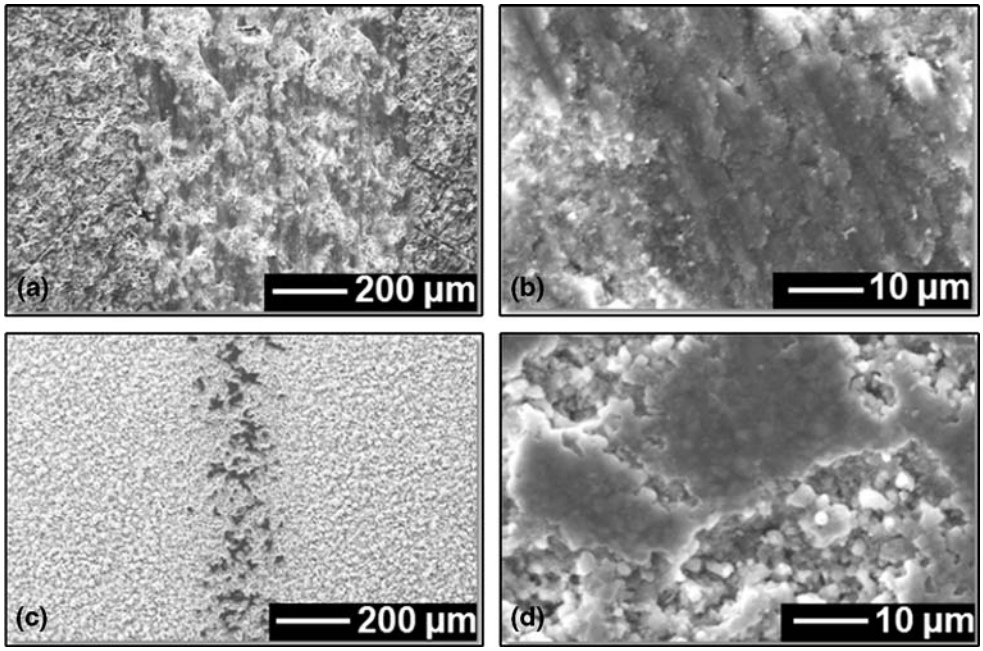

Fig. 8 Wear tracks for Al_2O_3 (a, b) micrometer-sized (APS) and (c, d) sub-micrometer-sized (SPS, spray distance = 30 mm) coatings (1500 m sliding distance following conditions specified in Sect 2.2)

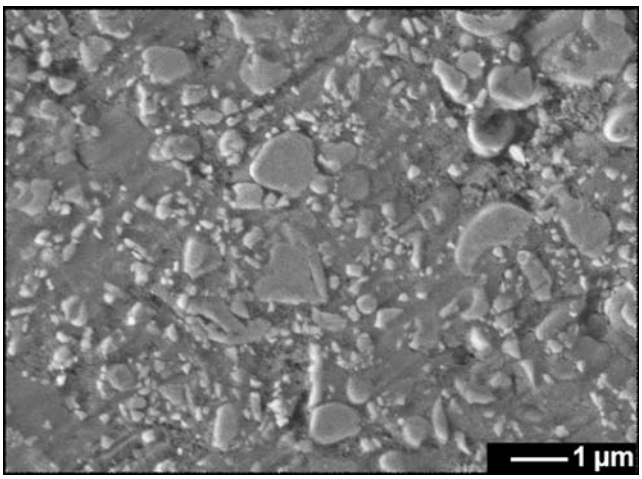

Fig. 9 Wear tracks (FESEM) of Al_2O_3 sub-micrometer-sized (SPS, spray distance = 30) coatings (1500 m sliding distance following conditions specified in Sect 2.2)

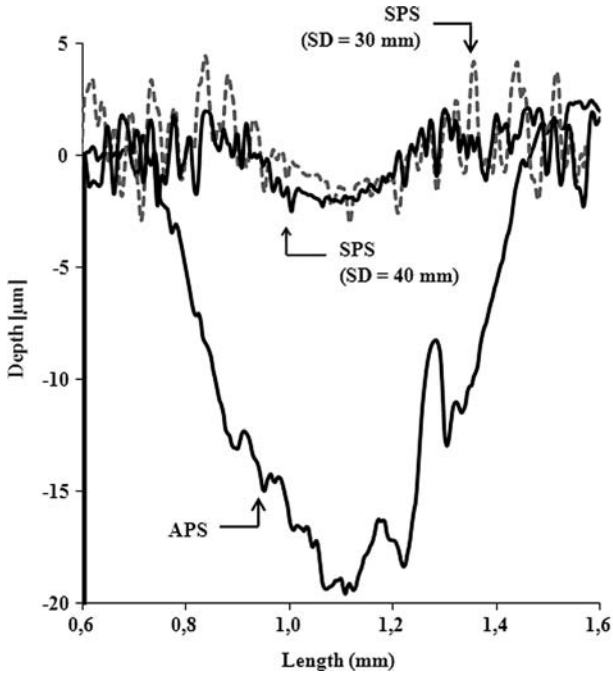

Fig. 10 Wear profiles for Al_2O_3 micrometer-sized (APS) and sub-micrometer-sized (SPS, spray distance = 30 and 40 mm) coatings (1500 m sliding distance following conditions specified in Sect 2.2)

4. Conclusions

This study highlights the improvement brought by the decrease in plasma spray coating structural scale on the coating friction coefficient.

The friction coefficient is decreased by a factor of two when the characteristic scale is reduced by two orders of magnitude. Accordingly, the wear resistance of SPS coatings is very significantly higher than APS coatings, thanks to a better toughness of the layer when shown by track view with plastic deformation. When considering different SPS coating architectures (resulting from different spray distances), the higher the cohesion, the lower the friction coefficient and the wear.

Acknowledgments

This work was conducted within the frame of the French FCE-NANOSURF consortium (Mecachrome, Frechin, CRT Plasma Laser, Cilas, CEA, CITRA) that is granted by the French Ministry and Industry and local governments of Région Centre and Limousin, the financial supports of which are acknowledged by the authors. The authors gratefully acknowledge the valuable help of Olivier Tingaud, SPCTS – UMR CNRS 6638.

References

1. Kyoto Protocol to the United Nations Framework Convention on Climate Change, United Nations, 1998
2. Intergovernmental Panel on Climate Change, Climate Change 2007, released November 17, 2007, Valencia, Spain
3. Y. Fukushima, M. Shimada, S. Kraines, M. Hirao, and M. Koyama, Scenarios of Solid Oxide Fuel Cell Introduction into Japanese Society, *J. Power Sources*, 2004, **131**, p 327-339
4. E. Broszeit, Mechanical, Thermal and Tribological Properties of Electro- and Chemodeposited Composite Coatings, *Thin Solid Films*, 1982, **2**(95), p 133-142
5. G. Barbezat, Coating for the Working Surface of the Cylinders of Combustion Engines and a Method of Applying such a Coating, US Patent 6,548,195B1, 2003
6. G. Barbezat, Surface Layer Forming a Cylinder Barrel Surface, a Spraying Powder Suitable Therefore and a Method of Creating such a Surface Layer, US Patent 6,578,539B2, 2003
7. Q. Feng, T. Li, H. Yue, K. Qi, F. Bai, and J. Jin, Preparation and Characterization of Nickel Nano-Al_2O_3 Composite Coatings by Sediment Co-Deposition, *Appl. Surf. Sci.*, 2008, **254**(8), p 2262-2268
8. R.S. Lima and B.R. Marple, Thermal Spray Coatings Engineered from Nanostructured Ceramic Agglomerated Powders for Structural, Thermal Barrier and Biomedical Applications: A Review, *J. Therm. Spray Technol.*, 2007, **16**(1), p 40-63
9. M. Gell, E.H. Jordan, Y.H. Sohn, D. Goberman, L. Shaw, and T.D. Xiao, Development and Implementation of Plasma Sprayed Nanostructured Ceramic Coatings, *Surf. Coat. Technol.*, 2001, **146-147**, p 48-54
10. E.H. Jordan, M. Gell, Y.H. Sohn, D. Goberman, L. Shaw, S. Jiang, M. Wang, T.D. Xiao, Y. Wang, and P. Strutt, Fabrication and Evaluation of Plasma Sprayed Nanostructured Alumina-Titania Coatings with Superior Properties, *Mater. Sci. Eng. A*, 2001, **301**(1), p 80-89
11. H. Chen, Y. Zhang, and C. Ding, Tribological Properties of Nanostructured Zirconia Coatings Deposited by Plasma Spraying, *Wear*, 2002, **253**(7-8), p 885-893
12. Y.-C. Zhu, K. Yukimura, C.-X. Ding, and P.-Y. Zhang, Tribological Properties of Nanostructured and Conventional WC-Co Coatings Deposited by Plasma Spraying, *Thin Solid Films*, 2001, **388**(1-2), p 277-282
13. J.H. Ouyang and S. Sasaki, Effects of Different Additives on Microstructure and High-Temperature Tribological Properties of Plasma-Sprayed Cr_2O_3 Ceramic Coatings, *Wear*, 2001, **249**, p 56-67
14. Coll, Used Lubricants. Pub. Agence de l'Environnement et de la Maîtrise de l'Energie, Angers, France, p 12 (in French)
15. P. Fauchais, V. Rat, C. Delbos, J.-F. Coudert, T. Chartier, and L. Bianchi, Understanding of Suspension DC Plasma Spraying of Finely Structured Coatings for SOFC, *IEEE Trans. Plasma Sci.*, 2005, **33**(2), p 920-930
16. H. Kassner, R.O. Siegert, D. Hathiramani, R. Vassen, and D. Stoever, Application of Suspension Plasma Spraying (SPS) for Manufacture of Ceramic Coatings, *J. Therm. Spray Technol.*, 2008, **17**(1), p 115-123
17. C. Delbos, "Contribution to the Understanding of Ceramic (Y-PSZ, perovskite, etc.) or Metallic (Ni, etc.) Particles Injection by a Liquid Carrier in a Plasma Jet to Manufacture Finely-Structured Coatings for SOFC," Ph.D. Thesis, University of Limoges, 2004 (in French)
18. J. Oberste Berghaus, J.-G. Legoux, C. Moreau, F. Tarasi, and T. Chráska, Mechanical and Thermal Transport Properties of Suspension Thermal-Sprayed Alumina-Zirconia Composite Coatings, *J. Therm. Spray Technol.*, 2008, **17**(1), p 91-104
19. O. Tingaud, R. Etchart-Salas, V. Rat, J.-F. Coudert, H. Ageorges, A. Grimaud, A. Denoirjean, P. Fauchais, G. Montavon, N. Caron, and S. Alexandre, *Suspension Plasma Spraying of Alumina Coatings: Process and Coating Structure*, Kyoto, Japan, Aug 26-31, 2007
20. G. Antou, G. Montavon, F. Hlawka, A. Cornet, and C. Coddet, Characterizations of the Pore-Crack Network Architecture of Thermal Sprayed Coatings, *Mater. Charact.*, 2004, **53**(5), p 361-372
21. S. Valette, G. Trolliard, A. Denoirjean, and P. Lefort, Iron/Wustite/Magnetite/Alumina Relationships in Plasma Coated Steel: A TEM Study, *Solid State Ionics*, 2007, **178**(5-6), p 429-437
22. ISO 4287:1997 Standard. Surface Texture: Profile Method – Terms, Definitions and Surface Texture Parameters
23. R.S. Lima and B.R. Marple, From APS to HVOF Spraying of Conventional and Nanostructured Titania Feedstock Powders: A Study on the Enhancement of the Mechanical Properties, *Surf. Coat. Technol.*, 2006, **200**(11), p 3428-3437
24. X. Lin, Y. Zeng, S.-W. Lee, and C. Ding, Characterization of Alumina-3 wt.% Titania Coating Prepared by Plasma Spraying of Nanostructured Powders, *J. Eur. Ceram. Soc.*, 2004, **24**(4), p 627-634
25. O. Tingaud, A. Grimaud, A. Denoirjean, G. Montavon, V. Rat, J.-F. Coudert, and P. Fauchais, Effects of Operating Parameters on SPS Alumina Coatings Structures to Manufacture Functionally-Graded Layers, *Surf. Coat. Technol.* (in press)
26. P.P. Psyllaki, M. Jeandin, and D.I. Pantelis, Microstructure and Wear Mechanisms of Thermal-Sprayed Alumina Coatings, *Mater. Lett.*, 2001, **47**(1-2), p 77-82
27. D.I. Pantelis, P. Psyllaki, and N. Alexopoulos, Tribological Behaviour of Plasma Sprayed Al_2O_3 Coatings Under Severe Wear Conditions, *Wear*, 2000, **237**(2), p 197-204
28. N.B. Dahotre and S. Naya, Nanocoatings for Engine Application, *Surf. Coat. Technol.*, 2005, **194**(1), p 404
29. H. Hahn, P. Mondal, and K. Padmanabhan, Plastic Deformation of Nanocrystalline Materials, *Nanostruct. Mater.*, 1997, **9**, p 603
30. X. Lin, Y. Zeng, C. Ding, and P. Zheng, Tribological Behaviour of Nanostructured Al_2O_3-3 wt% TiO_2 Coating Against Steel in Dry Sliding, *Tribol. Lett.*, 2004, **17**(1), p 19-26
31. J. Zhang, J. He, Y. Dong, X. Li, and D. Yan, Microstructure and Properties of Al_2O_3-13%TiO_2 Coatings Sprayed Using Nanostructured Powders, *Rare Met.*, 2007, **26**(4), p 391-397
32. Y. Wang, S. Jiang, M. Wang, S. Wang, T.D. Xiao, and P.R. Strutt, Abrasive Wear Characteristics of Plasma Sprayed Nanostructured Alumina/Titania Coatings, *Wear*, 2000, **237**(2), p 176-185